Polymorphic uncertainty in met-ocean conditions and the influence on fatigue loads

Polymorphic uncertainty in met-ocean conditions and the influence on fatigue loads

Clemens Hübler, Franziska Müller, and Raimund Rolfes

Institute of Structural Analysis, Leibniz Universität Hannover, ForWind, Appelstr. 9a, D-30167 Hannover, Germany

E-mail: c.huebler@isd.uni-hannover.de

Abstract. An accurate numerical simulation of the structural lifetime of offshore wind turbines is a challenging task due to several reasons. One of them is the uncertainty of met-ocean conditions acting on a turbine, e.g. wind and waves. This uncertainty can be divided into two kinds of uncertainty: aleatory and epistemic uncertainty. If both types of uncertainty occur, this is called polymorphic uncertainty. According to the state of the art, for met-ocean conditions, mainly aleatory uncertainty is considered or both types of uncertainty are modelled using a single probability density function. This leads to a simplification of the actual uncertainty, whose effect on the lifetime estimation has not been analysed so far. In that sense, in this work, the influence of various uncertainty models for met-ocean conditions on long-term damage equivalent loads (DELs) – representing the wind turbine fatigue lifetime – is investigated. For this purpose, different uncertainty models for met-ocean conditions are derived using real measurement data. Not only purely probabilistic models are applied, but imprecise probabilities - here interval random variables - as well. It is shown that the uncertainty models have a considerable influence on the fatigue life of offshore wind turbines. Especially, the large fatigue load intervals, which are determined, clarify the importance of a well-founded decisions regarding uncertainty modelling of met-ocean conditions.

1. Introduction

Although the share of offshore wind energy in the overall energy production has been steadily growing over the last years, the cost of offshore wind energy is still high compared to other renewable energies [1]. To drive the cost of offshore wind energy further down, an increase or at least a better knowledge of the reliability of the turbine is beneficial. Since the design of offshore wind turbines - especially of steel components - is mainly governed by the fatigue lifetime [2], an accurate and reliable estimation of fatigue loads is required. The uncertainty of fatigue loads is mostly influenced by uncertain met-ocean conditions, like the wind speed or the wave height [3, 4]. However, it is not straightforward to determine the uncertainty of these reliability-determining met-ocean conditions. First, they feature some amount of inherent, physical randomness. This uncertainty is called aleatory uncertainty. It is not reducible. Usually, it is modelled using probabilistic approaches, i.e. probability density functions [5]. Second, to determine these probability distributions, measurements are required. These measurements feature their own uncertainty (measurement uncertainty). They are limited (uncertainty due to a lack of data). Moreover, statistical distributions are used to fit the empirical ones. This leads to uncertainty of the statistical model. Hence, another type of uncertainty should be

included in an accurate uncertainty model for met-ocean conditions. It is called epistemic uncertainty. Epistemic uncertainty is reducible, e.g. by gathering more data. It can, for example, be modelled by interval or fuzzy variables [6]. If both types of uncertainty occur, this is called polymorphic uncertainty [5]. Polymorphic uncertainty can be modelled using imprecise probabilities. However, according to the state of the art, for met-ocean conditions, mainly aleatory uncertainty is considered [7, 9]. If polymorphic uncertainty is taken into account, purely probabilistic approaches are used, for example, by averaging different distributions [10]. However, using purely probabilistic approaches, a separated analysis of both types of uncertainty is not possible. Both approaches are simplifications of the actual uncertainty, whose effects on fatigue loads has not been analysed so far.
More accurate uncertainty models for polymorphic uncertainty are based on imprecise probabilities [6]. Here, for example, interval random variables, also called p-boxes, or fuzzy random variables are adequate models. For interval random variables, the determination of probability distributions and the corresponding intervals using real measurement data is described, for example, by Zhang et al. [11]. In that sense, in this work, the influence of more accurate uncertainty models for met-ocean conditions on fatigue loads is investigated. Here, interval random variables are used to represent the uncertainty.
For this purpose, first, different uncertainty models are derived to represent the most relevant met-ocean conditions (wind speed, wave height, and wave period). For example, pure probabilistic representations using theoretical and empirical distributions are applied. To be more accurate, in addition, polymorphic uncertainty is modelled using interval random variables based on confidence intervals. Second, lifetime damage equivalent loads (DELs; c.f. Dimitrov et al. [12]), representing the fatigue lifetime of a turbine, are calculated for all uncertainty models. Since the calculation of lifetime DELs is computational demanding, a meta-model-based approach is applied [12, 13]. Finally, resulting DELs for different uncertainty models are compared. Conclusions are drawn.

2. Uncertainty models

2.1. Met-ocean data

In this study, uncertainty models for three relevant met-ocean conditions - namely wind speed, wave height and wave period - are derived directly from offshore measurement data. The prominent relevance of these three conditions was identified within previous studies [3, 4]. The raw data is taken from the FINO3 platform [14]. Distributions (including correlations and interval definitions) are determined. The FINO3 measurement mast is located in the North Sea. Inter alia, maximum, minimum, mean, and standard deviation values of the wind speed, measured at different heights between 30 m and 100 m above mean sea level, are available for 10-minute intervals. Wind speeds are measured with cup and ultrasonic anemometers. In this study, cup anemometers are used. Three anemometers are installed around the mast to minimise shadow effects. A buoy in the immediate vicinity of the research platform (about 150 m) measures wave conditions. For example, mean values of significant wave heights and wave peak periods are recorded every 30 minutes. The FINO3 platform has been measuring continuously since 2009. Here, a measurement period of 8 years (1^{st} Dec. 2010 to 30^{th} Nov. 2018) is considered. More detailed information regarding the measurements at FINO3 can be found, for example, on the website [14]. The post-processing of the raw data, e.g. the reduction of tower shadow effects, is described in Hübler et al. [7].
Since met-ocean conditions are not independent of each other, correlations between inputs have to be considered. In this work, wind speed is regarded as an independent input. Wave heights depend on wind speeds. For example, during a storm, not only high wind speeds occur, but the probability for a rough sea with high waves is increased as well. Moreover, wave periods depend on the wave height. A trend of longer periods for higher waves can be observed. Both

dependencies can be seen in Figure 1. It shows scatter plots of measured mean values at FINO3 within the eight year period. This description of the dependencies of the three environmental conditions is fairly simplified. Different physical reasons for sea states are not considered. For example, there is no differentiation between wind sea waves (created by local wind) and swell waves (created by distant storms). As indicated by colour highlighting in Figure 1 and the illustration of the dependencies between the environmental conditions in Figure 2, a more sophisticated description could be beneficial. Nonetheless, since the following analyses are based on statistical methods, even using a highly simplified description, an accurate representation of the real sea conditions is possible. This is demonstrated later on in Figure 4 and 5 and by the small differences of the approaches *Emp* and *Theo* in Table 1. Therefore, this simplification of the sea state modelling is justified for the present case.

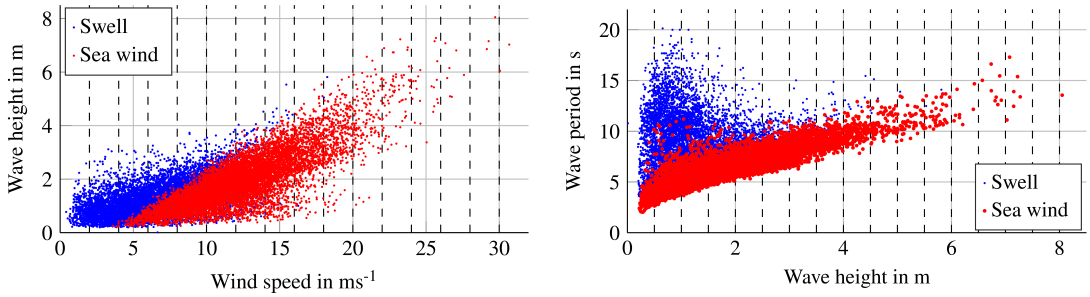

Figure 1. Scatter plots of the measured mean values at FINO3 within the eight year period to illustrate dependencies. Differentiation between swell and wind sea according to the wave age [8]. Left: wind speed vs. wave height. Right: wave height vs. wave period.

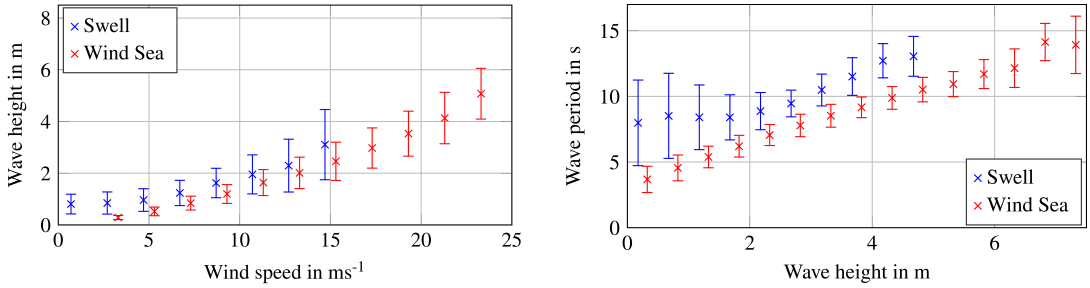

Figure 2. Development of mean values (crosses) and standard deviations (error bars) of depending environmental conditions in different bins and different conditions (swell and wind sea). Left: wind speed vs. wave height. Right: wave height vs. wave period.

To cover the described dependencies within the uncertainty models, the data is divided into bins. This means: For the wind speed, the entire wind speed data is utilised to determine the uncertainty model. However, for the wave height, the data is divided into bins of $2\,\mathrm{m\,s^{-1}}$ wind speed (marked in Figure 1). For each bin, an individual uncertainty model is constructed. Similarly, for the wave period, the data is split up into bins of 0.5 m wave height. This approach of including dependencies between met-ocean conditions, was already successfully applied in Hübler et al. [7]. There, additional explanations can be found.

2.2. Theory

In general, there are various methods to model input uncertainty. Examples are random variables, interval variables, fuzzy probability-based random variables, etc. [5]. In this work, the focus is on random variables and interval random variables (i.e. p-boxes). The first approach is the standard method for aleatory uncertainty. It is applied, for example, by Stewart et al. [10] or Fischer et al. [9]. The latter one enables to model - in addition to the aleatory uncertainty - epistemic uncertainty explicitly. This is helpful, if, for example, probability density functions cannot be determined precisely. In this case, the additional interval definition can cover the uncertainty due to incomplete or imprecise data. Fuzzy random variables - not considered in this work - would be an alternative [15]. Overall, five different methods are compared in this work. The first two are based on random variables. Either empirical cumulative density functions (CDFs) are applied (approach 1: *Emp*) or the best fitting theoretical CDF is determined (approach 2: *Theo*). Approaches three to five are p-boxes, i.e. intervals of CDFs are used. Again, there is an empirical interval approach (approach 3: *EmpInt*) that is based on Kolmogorov-Smirnov confidence intervals. For the last two concepts, theoretical CDFs are determined. However, the determination of theoretical CDFs cannot be completely exact. The resulting epistemic uncertainty can either be represented by applying intervals for the distribution parameters (approach 4: *ParamInt*) or by creating an envelope of various potentially suitable CDFs, i.e. using different theoretical distributions (approach 5: *DistrInt*). All p-box approaches are described in more detail by Zhang et al. [11]. The theory of all five methods is briefly summarised in the following. The resulting distributions and illustrations of them can be found in the next section.

Emp: The empirical CDF can be determined by relating the number of data points (x_i) that exceeds x to the overall number of data points n:

$$F_{Emp}(x) = \frac{1}{n} \sum_{i=1}^{n} \mathbf{1}_{x_i \leq x}(x), \tag{1}$$

where $\mathbf{1}_{x_i \leq x}$ is the indicator function that is equal to one for $x_i \leq x$ and equal to zero in all other cases.

Theo: For the best fitting theoretical CDF, first, several theoretical probability functions are fitted to the empirical CDF. In the present case, for example, normal distributions, Gumbel distributions, etc. are fitted. Distribution parameters (e.g. μ and σ for the normal distribution) are determined using a maximum likelihood estimation. Since several distributions are fitted, in a second step, $\mathcal{X}^2$ tests are conducted to determine which theoretical probability function resembles the empirical one most. For more details, it is referred to Hübler et al. [7], where this procedure was already applied to similar data. For the wind speed, this procedure yields a Weibull distribution with $\lambda = 0.0920$ and $k = 2.2747$:

$$F_{Theo}(x) = 1 - e^{-(\lambda x)^k}. \tag{2}$$

For the wave height, Gumbel and gamma distributions are found to be best suitable depending on the wind speed bin. For the wave period, bi-modal Gumbel distributions are selected independent of the wave height bin (cf. Hübler et al. [7]).

EmpInt: Since empirical CDFs are uncertain, for example, due to a limited number of data points, a lower ($\underline{F}_{Emp}(x)$) and an upper ($\bar{F}_{Emp}(x)$) empirical CDF can be defined as follows:

$$\underline{F}_{Emp}(x) = \min(1, \max(0, F_{Emp}(x) - D_n^{\alpha})) \quad \text{and} \tag{3}$$

$$\bar{F}_{Emp}(x) = \min(1, \max(0, F_{Emp}(x) + D_n^{\alpha})), \tag{4}$$

where D_n^{α} is the critical value in a Kolmogorov-Smirnov test at the significance level α and a sample size n. In this work, a standard value of $\alpha = 0.05$ is used. Lower values for α yield

higher uncertainties and therefore wider intervals.
ParamInt: Similar to the interval definition for the empirical CDF, intervals can be defined for the theoretical distribution as well. Here, the approach is that the determined distribution parameters θ, e.g. $\theta = (\lambda, k)$ for the Weibull distribution, are uncertain themselves. Hence, it is convenient to define intervals for them: $\left[\underline{\theta}, \bar{\theta}\right]$. Using these interval definitions, lower and upper CDFs can be defined:

$$\underline{F}_{Theo}(x) = \min(F_{Theo}(x|\theta)) \quad \text{with} \quad \underline{\theta} \leq \theta \leq \bar{\theta} \quad \text{and} \tag{5}$$

$$\bar{F}_{Theo}(x) = \max(F_{Theo}(x|\theta)) \quad \text{with} \quad \underline{\theta} \leq \theta \leq \bar{\theta}. \tag{6}$$

To be in line with the empirical interval CDF, intervals of the distribution parameters correspond to the 95 % confidence interval.
It should be noted that the minimising and maximising problem can be greatly simplified by just using the limits of θ, i.e. $\underline{\theta}$ and $\bar{\theta}$, since they lead to the extreme values for a given probability function.
DistrInt: Alternatively, the uncertainty in determining the theoretical distribution can be attributed to the distribution itself instead of to its parameters. In this case, not only the best fitting distribution according to the $\mathcal{X}^2$ tests is selected, but m different types of distributions $F_{Theo,i}$. For each type of distribution, the distribution parameters are determined. Here, we abstain from assuming an additional uncertainty of distribution parameters. Nevertheless, a combination of parameter uncertainty with distribution uncertainty could be subject of future work. Lower and upper CDFs are constructed by finding the minimum and maximum CDF for each point x:

$$\underline{F}_{Distr}(x) = \min(F_{Theo,i}(x)) \quad \text{for} \quad i = 1, \ldots, m \quad \text{and} \tag{7}$$

$$\bar{F}_{Distr}(x) = \max(F_{Theo,i}(x)) \quad \text{for} \quad i = 1, \ldots, m. \tag{8}$$

2.3. Resulting uncertainty models

The approaches presented in the previous section are applied to determine different uncertainty models for wind speed, wave height, and wave period based on FINO3 measurement data (c.f. Section 2.1). As stated before, wind speed is considered to be the independent variable. Hence, all wind speed data is taken into account. For wave inputs, different uncertainty models are built up for different bins. Apart from that the procedure is the same for all three inputs. Exemplary, the identified wind speed CDFs are shown in Figure 3. In addition, a detailed view of theses CDFs is given to see the differences more clearly. Lastly, the wave height CDFs for the wind speed bin 16 m s^{-1} to 18 m s^{-1} are presented as well.
Several facts become clear when analysing the results presented in Figure 3. First, for the wind speed, the uncertainty models are quite similar. A detailed view is needed to spot differences. Only the use of different distributions (*DistrInt*) leads to a more widely spread interval. The reason for this good match of all models is the well fitting representation of the real data by theoretical distributions. In addition, the large amount of data reduces statistical uncertainties. For the dependent variable - here the wave height, less data is available, since the data is split up into bins. Hence, statistical uncertainty increases. Differences between uncertainty models become more obvious. For the empirical interval, it should be noted that the definition in equations (3) and (4) lead to a "vertical" distance of the upper ($\bar{F}_{Emp}(x)$) and lower limit ($\underline{F}_{Emp}(x)$) to the empirical one ($F_{Emp}(x)$), e.g. $\bar{F}_{Emp}(x) = F_{Emp}(x) + D_n^{\alpha}$. Hence, for $x \to \infty$ or $x \to -\infty$, this results in limits that do not converge to 0 or 1, but to $1 - D_n^{\alpha}$ or D_n^{α}, respectively. This fact would be problematic in the following, as, for example, $\underline{F}_{Emp}^{-1}(1) = \infty$. To resolve this fact, maximum distances to the empirical distribution in "horizontal" direction of 5 m s^{-1}, 2 m, and 3 s for wind speed, wave height and period, respectively, are defined. This yields, for

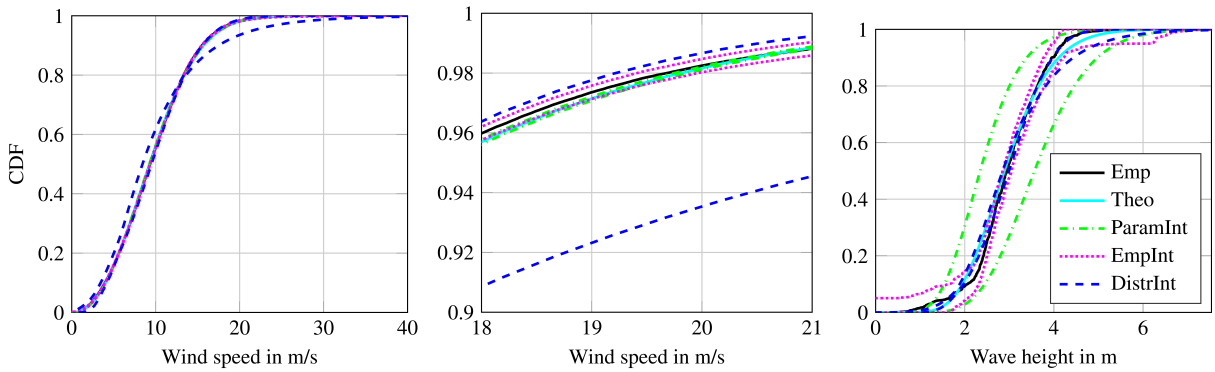

Figure 3. Illustration of different uncertainty models: Left: wind speed. Middle: detailed view for wind speed. Right: wave height for the wind speed bin $16\,\mathrm{m\,s^{-1}}$ to $18\,\mathrm{m\,s^{-1}}$.

example, $F^{-1}_{Emp}(1) = F^{-1}_{Emp}(1) + 2\,\mathrm{m}$ for the wave height. This extra criterion can be spotted in Figure 3 (right) as a kinking point of the *EmpInt* curve just above 6 m. In general, the choice of the specific values for the maximum distances is arbitrary. For this work, several maximum values were tested in advance. Too high values lead to pronounced kinking points. Such non-smooth distributions are normally not physical. Too low values narrow the interval. Hence, the actual epistemic uncertainty would be underestimated. In any case, the choice of these values affects mainly the lower and upper tails of the CDFs. Since fatigue is determined by the large amount of data points close to the mean, the effect on the overall uncertainty model is not critical.

To demonstrate the performance of the uncertainty models, especially of the input dependencies, in Figure 4 and 5, the scatter of the original data is compared to the scatter of realisations based on the theoretical uncertainty model (*Theo*). Clearly, the general trend is represented well (c.f. Figure 5). Some differences can be spotted for "extreme values". For those extremes, theoretical distributions might predict too high values. This limited accordance for the tails of the distributions is well-known. It can be explained by the higher weighting of the region close to the mean value for the fitting. However, as explained before, this deviation is fairly unproblematic for fatigue loads.

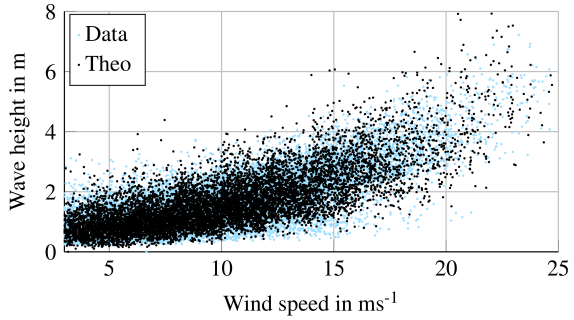

Figure 4. Comparison of the scatter of the original wind-wave data to the prediction by the theoretical uncertainty model (*Theo*).

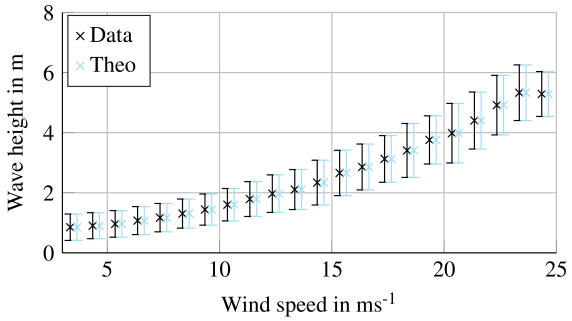

Figure 5. Wave height mean values (crosses) and standard deviations (error bars) in different $1\,\mathrm{m\,s^{-1}}$ wind speed bins.

3. Fatigue load calculation

To efficiently determine the influence of uncertainty models on wind turbine fatigue loads, three aspects have to be considered. First, a procedure to calculate fatigue loads or at least a measure for fatigue is needed. Here, lifetime DELs [12] are utilised. Second, a suitable wind turbine model is required. Such a turbine is the NREL 5 MW reference wind turbine [16]. And last, to ensure an efficient computation, a meta-model, which correlates polymorphic uncertain met-ocean conditions to short-term DELs, is helpful. All three aspects are explained in more detail in the following.

3.1. Damage equivalent load

A short-term DEL represents a load signal with a constant frequency and amplitude (S_{eq}) yielding the same damage according to the Palmgren-Miner rule as an investigated (realistic) short-term load signal with various frequencies and amplitudes (S_i):

$$S_{\mathrm{eq}} = \left(\sum \frac{n_i S_i^m}{N_{\mathrm{ref}}} \right)^{-m}, \tag{9}$$

where $N_{\mathrm{ref}} = 600$ to set the frequency of the DEL to 1 Hz for a 10-minute period. S_i and n_i are the different amplitudes and the corresponding number of cycles in the original load signal, when applying a rainflow counting. The material exponent is chosen as $m = 3$ for steel.
For long-term fatigue loads, a lifetime DEL [12] can be defined:

$$S_{\mathrm{eq,LT}} = \left(\int S_{\mathrm{eq}}(\mathbf{x})^m f(\mathbf{x}) d\mathbf{x} \right)^{-m}, \tag{10}$$

where $\mathbf{x}$ is the input vector and $f(\mathbf{x})$ is the joint probability density function of $\mathbf{x}$. Since this integral cannot be solved analytically, normally, a finite number of random realisations of $\mathbf{x}$ is used to estimate $S_{\mathrm{eq,LT}}$, i.e. Monte Carlo integration.
For uncertainty models with interval random variables $[\underline{\mathbf{x}}, \bar{\mathbf{x}}]$, the lifetime DEL is also an interval $\left[\underline{S}_{\mathrm{eq,LT}}, \bar{S}_{\mathrm{eq,LT}}\right]$. Due to the fact that $\underline{\mathbf{x}}$ does not necessarily yield $\underline{S}_{\mathrm{eq,LT}}$, for each realisation of $\mathbf{x}$, the minimum and the maximum value of S_{eq} has to be found, e.g.:

$$\underline{S}_{\mathrm{eq}}(\mathbf{x}) = \min \left(S_{\mathrm{eq}}(\mathbf{x}) | \mathbf{x} \in [\underline{\mathbf{x}}, \bar{\mathbf{x}}] \right). \tag{11}$$

In this work, the minimisation problem is solved by applying a global pattern search approach [17]. A track number of $T = 2$ is chosen. A low track number results in a fairly local version of the global pattern search approach. This is reasonable, since there is only a low number of local minima in the "truncated" objective spaces, i.e. the objective spaces resulting from the interval definitions.
Descriptively, for interval random variables, this means that each realisation $\mathbf{x}$ is no longer represented by a single point, but by a (set of) multi-dimensional rectangle(s). For ten exemplary realisations and the distribution interval (*DistrInt*), the corresponding search spaces are illustrated in Figure 6. The shown rectangles represent the limits of the input variables $[\underline{\mathbf{x}}, \bar{\mathbf{x}}]$, in which we search for maximum and minimum lifetime DELs ($\underline{S}_{\mathrm{eq,LT}}$ and $\bar{S}_{\mathrm{eq,LT}}$). Just a point of clarification, in Figure 6, only ten realisations are shown. This is only for illustration purposes. For the calculation, thousands of representative realisations are used. This corresponds to the thousands of points (*Theo*) in Figure 4. Each point for a probabilistic approach (e.g. *Theo*) corresponds to a (set of) multi-dimensional rectangle(s) for an interval random approach (e.g. *DistrInt*). This feature is illustrated in Figure 7. It shows for five exemplary realisations the values for the theoretical uncertainty model (*Theo*) and the corresponding rectangles for the interval approach (*DistrInt*). The five realisations are highlighted in different colours. In Figure

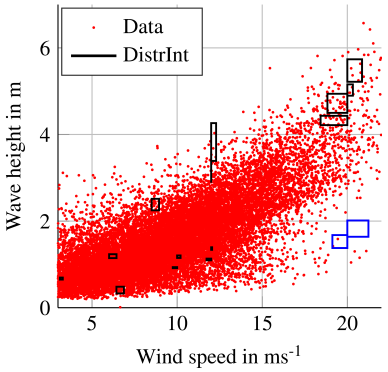

Figure 6. Illustration of the search space for the distribution interval (*DistrInt*) for 10 exemplary realisations of $\mathbf{x}$.

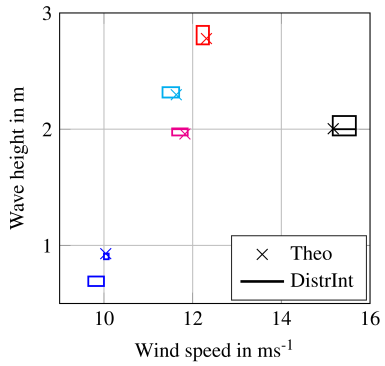

Figure 7. Illustration of corresponding search space (*DistrInt*) for point realisations (*Theo*) for 5 realisations.

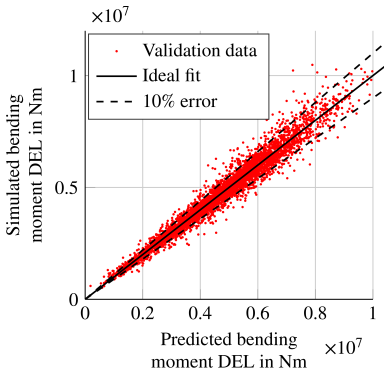

Figure 8. Visual validation of the Kriging model: Kriging prediction vs. aero-elastic simulation results.

6, thousands of rectangle would not be illustrative. Hence, we abstained from showing all realisations for the interval approach.
It might be apparent that more than ten (five) rectangles can be spotted in Figure 6 (Figure 7). This is due to the fact that the wave height definitions differ within the corresponding wind speed bins. For example, the two adjacent rectangles at a wind speed of approximately 20 m s^{-1} and a wave height of around 1.5 m (marked in blue in Figure 6) represent only a single search space, i.e. one realisation of $\mathbf{x}$. In general, the limits are wider in case of "extreme" events, where less data is available.

3.2. Wind turbine model

To determine the short-term DELs in equation (9), load signals are required. According to the state of the art, these are determined by conducting time-domain simulations using aero-elastic simulation codes. In this work, the NREL 5 MW reference wind turbine with the OC3 monopile as substructure [18] is simulated using the aero-hydro-servo-elastic simulation framework FASTv8 [19] of the "National Renewable Energy Laboratory" (NREL). A soil model that applies soil-structure interaction matrices [20, 21] enhances the FASTv8 code. Soil conditions of the OC3 phase II model [18] are assumed. For all simulations, the simulation length is set to 10 minutes according to Hübler et al. [7]. The "run-in" time (i.e. the time that has to be removed from each time series to exclude initial transients) is set to 240 seconds. According to Hübler et al. [7], this "run-in" time should be sufficient, if initial conditions - e.g. for the rotor speed - are used, which is done in this study. The turbulent wind field is calculated using the Kaimal model. The JONSWAP spectrum is applied to compute irregular waves. These spectra might not be consistent with the derived long-term distributions (c.f. Section 2.3). However, they follow the state of the art and the recommendations in current standards [23]. Moreover, the accuracy of the aero-elastic simulations is not focus of this work. Only one load is considered exemplary: the overturning moment in wind direction at mudline. For future work, it is definitely necessary to consider all design-driving loads. However, in this work, the intension is a more exemplary illustration of the effects of polymorphic uncertainty modelling.

3.3. Meta-modelling

For the determination of long-term DELs, according to equation (10), a multi-dimensional integration is required. As stated before, this integral is normally approximated by a finite number of random realisation of $\mathbf{x}$. Ideally, the number of realisations is 1.3149×10^6. This is the number of 10-minute periods in the entire lifetime of 25 years. If this number of realisations is used, no load extrapolation techniques - adding additional uncertainties - are required. Moreover, for interval random variables, for each realisation, an optimisation has to be conducted (cf. Section 3.1). This leads to approximately 10^8 to 10^9 overall model evaluations. Considering the fact that one model evaluation (one realisation of $S_{\mathrm{eq}}(\mathbf{x})$), i.e. one time domain simulation, has a computing time of approximately 10 minutes, this procedure becomes inappropriate. Therefore, a meta-model, which approximates $S_{\mathrm{eq}}(\mathbf{x})$, is used in this work. This procedure yielded promising results in the past [12, 24]. Based on results of Müller et al. [13], a Kriging meta-model with a linear basis function and a squared exponential covariance function is set up. The Kriging model is fitted based on $n_{\mathrm{training}} = 5000$ random realisations of $\mathbf{x}$ as training data points. It is validated based on another $n_{\mathrm{test}} = 5000$ test data points. A visual validation can be seen in Figure 8. Moreover, the normalised root-mean-square error for the test data is:

$$\mathrm{NRMSE} = \frac{1}{\mathrm{E}(S_{\mathrm{eq}}(\mathbf{x}))} \sqrt{\frac{\sum_{i=1}^{n_{\mathrm{test}}} (\hat{S}_{\mathrm{eq}}(\mathbf{x}_i) - S_{\mathrm{eq}}(\mathbf{x}_i))^2}{n_{\mathrm{test}}}} = 0.075, \tag{12}$$

where $\hat{S}_{\mathrm{eq}}(\mathbf{x})$ is the predicted short-term DEL by the Kriging model. Clearly, there are possible improvements regarding the meta-modelling (see for example Dimitrov et al. [12]). Moreover, in any case, meta-modelling adds an additional uncertainty to the lifetime DEL calculation. However, both is not focus of this work. Therefore, both is not further investigated.

4. Resulting fatigue loads

For each of the five uncertainty models, lifetime DELs (or lifetime DEL intervals) are calculated. Lifetime DELs are based on 1.3149×10^6 realisations of met-ocean conditions. Hence, the full turbine lifetime is calculated. Results are summarised in Table 1. For non-interval methods (*Emp* and *Theo*), the lifetime DEL is calculated ten times to show the low uncertainty of the lifetime DEL due to different met-ocean realisations over the entire turbine life. Hence, differences between uncertainty models are actually a result of the model and not of different random realisations.

On the one hand, the results in Table 1 demonstrate that pure probabilistic uncertainty models lead to quite similar results. This means that neither different met-ocean realisations over the entire turbine lifetime lead to significant differences (cf. $\sigma_{S_{\mathrm{eq,LT}}}$ in Table 1) nor does the change of the uncertainty model result in pronounced variations of the lifetime DEL (cf. *Emp* and *Theo*

Table 1. Resulting lifetime DELs for different uncertainty models. For non-interval models, mean values $\mu_{S_{\mathrm{eq,LT}}}$ and standard deviations $\sigma_{S_{\mathrm{eq,LT}}}$ of ten realisations are given.

Uncertainty model	$\mu_{S_{\mathrm{eq,LT}}}$ in MNm	$\sigma_{S_{\mathrm{eq,LT}}}$ in $(\mathrm{MNm})^2$	$\underline{S}_{\mathrm{eq,LT}}$ in MNm	$\bar{S}_{\mathrm{eq,LT}}$ in MNm
Emp	5.286	0.0018	–	–
Theo	5.287	0.0019	–	–
EmpInt	–	–	4.924	5.839
ParamInt	–	–	4.775	5.995
DistrInt	–	–	4.494	6.238

in Table 1). To be more precise, the differences of the two models are even within the range that can be explained by different realisations (i.e. $|\mu_{S_{\mathrm{eq,LT},Emp}} - \mu_{S_{\mathrm{eq,LT},Theo}}| < \sigma_{S_{\mathrm{eq,LT},Emp}}$). Hence, it is possible to represent the probabilistic behaviour with theoretical distributions with a good agreement. As a result, the choice of the probabilistic uncertainty model is of minor importance. However, on the other hand, the consideration of polymorphic uncertainty - being the focus of the work - yields wide ranges of lifetime DELs. Hence, it can be suspected that lifetime DELs exhibit a relevant amount of uncertainty, which is not detected by pure probabilistic approaches. As a result, pure probabilistic approaches can under- and overestimate real lifetime DELs. However, it has to be noted that the resulting interval of the lifetime DEL is significantly influenced by the interval method. That is why intervals for polymorphic uncertainty models have to be chosen with care. So far, it is not clear which interval random variable model is the most realistic one. Though, it can be assumed that *DistrInt* might overestimate the range of $S_{\mathrm{eq,LT}}$ due to the consideration of non-optimal distributions. *DistrInt* yields large intervals even for the wind speed (cf. Figure 3).

5. Conclusion and outlook

In this work, the influence of different uncertainty models - including polymorphic uncertainty - for met-ocean conditions on the fatigue loads (lifetime DELs) of offshore wind turbines was investigated. It was demonstrated that purely probabilistic approaches lead to quite similar results. However, the consideration of statistical uncertainty by applying interval random variables yields large ranges of lifetime DELs. This clarifies the existing uncertainty in fatigue loads that is neglected by using pure probabilistic approaches. Hence, probabilistic approaches can under- and overestimate the real fatigue lifetime of offshore wind turbines.

It has to be mentioned that several assumptions were made for this first study regarding polymorphic uncertain met-ocean conditions in wind turbine modelling. In that sense, it also has its limitations. For example, the uncertainty of the meta-model is not considered at all. Moreover, only three met-ocean conditions based on the data of one site are analysed. Similarly, regarding the outputs, the focus is on a single fatigue load and location: the overturning moment in wind direction at mudline. For other DELs, effects of the uncertainty modelling might be different. For example, for blade loads, wave loads - exhibiting high statistical uncertainty - are less relevant. This might result in more narrow intervals for blade fatigue loads.

This work represents only a first step towards the application of polymorphic uncertainty in wind turbine modelling. Since the relevance of polymorphic uncertainty modelling was successfully demonstrated, future work should address, inter alia, the inclusion of the meta-model uncertainty (cf. Figure 8). Moreover, fuzzy random uncertainty models might be interesting. Finally, it might be useful to improve the efficiency of the present approach. This can be achieved by having a closer look on the optimisation process for interval variables. This becomes especially relevant, if fuzzy random variables are used. In this case, optimisations have to be repeated for different α levels.

Acknowledgments

We gratefully acknowledge the financial support of the Deutsche Forschungsgemeinschaft (DFG, German Research Foundation) for the *ENERGIZE* project (436547100) and the Leibniz University Hannover for the *MetaWind* project within the program “Leibniz Young Investigator Grants”.

References

[1] IRENA 2019, Renewable Power Generation Costs in 2018. International Renewable Energy Agency.
[2] Moriarty PJ, Holley WE and Butterfield SP 2004, Extrapolation of extreme and fatigue loads using probabilistic methods. National Renewable Energy Lab., NREL/TP-500-34421.

[3] Hübler C, Gebhardt CG and Rolfes R 2017. Hierarchical four-step global sensitivity analysis of offshore wind turbines based on aeroelastic time domain simulations. *Renewable Energy* **111** 878-891.
[4] Hübler C, Gebhardt CG and Rolfes R 2019. Assessment of Sensitivity Analysis Methods of Different Complexity for Offshore Wind Turbines. *Proceedings of the 29th European Safety and Reliability Conference*, September 22-26, 2019, Hanover, Germany.
[5] Graf W, Götz M and Kaliske M 2015. Analysis of dynamical processes under consideration of polymorphic uncertainty. *Structural Safety* **52** 194-201.
[6] Beer M, Ferson S and Kreinovich V 2013. Imprecise probabilities in engineering analyses. *Mechanical Systems and Signal Processing* **37** 4-29.
[7] Hübler C, Gebhardt CG and Rolfes R 2017. Development of a comprehensive database of scattering environment conditions and simulation constraints for offshore wind turbines. *Wind Energy Science* **2** 491-505.
[8] Semedo A 2018. Seasonal Variability of Wind Sea and Swell Waves Climate along the Canary Current: The Local Wind Effect. *Journal of Marine Science and Engineering* **6** 28.
[9] Fischer T, De Vries WE and Schmidt B 2010. UpWind Design Basis (WP4: Offshore foundations and support structures). Endowed Chair of Wind Energy at the Institute of Aircraft Design Universität Stuttgart.
[10] Stewart GM, Robertson A, Jonkman J and Lackner MA 2016. The creation of a comprehensive metocean data set for offshore wind turbine simulations. *Wind Energy* **19** 1151-1159.
[11] Zhang H, Dai H, Beer M and Wang W 2013. Structural reliability analysis on the basis of small samples: an interval quasi-Monte Carlo method. *Mechanical Systems and Signal Processing* **37** 137-151.
[12] Dimitrov NK, Kelly MC, Vignaroli A and Berg J 2018. From wind to loads: wind turbine site-specific load estimation with surrogate models trained on high-fidelity load databases. *Wind Energy Science* **3** 767-790.
[13] Müller F, Hübler C and Rolfes R 2019. Well-founded meta modeling of wind turbines. *Proceedings of the 15th EAWE PhD Seminar on Wind Energy*, October 29-31 , 2019, Brussels, Belgium.
[14] https://www.fino3.de/en/
[15] Götz M 2017. Numerische Entwurfsmethoden unter Berücksichtigung polymorpher Unschärfe. PhD Thesis, TU Dresden.
[16] Jonkman J, Butterfield S, Musial W and Scott G 2009. Definition of a 5-MW reference wind turbine for offshore system development. National Renewable Energy Lab., NREL/TP-500-38060.
[17] Hofmeister B, Bruns M and Rolfes R 2019. Finite element model updating using deterministic optimisation: A global pattern search approach. *Engineering Structure* **195** 373-381.
[18] Jonkman JM and Musial W 2010. Offshore Code Comparison Collaboration (OC3) for IEA Task 23 Offshore Wind Technology and Deployment. National Renewable Energy Lab., NREL/TP-5000-48191.
[19] Jonkman J 2013. The New Modularization Framework for the FAST Wind Turbine CAE Tool. *51st AIAA Aerospace Sciences Meeting, including the New Horizons Forum and Aerospace Exposition*, January 7-10, 2013, Dallas, Texas, US.
[20] Häfele J, Hübler C, Gebhardt CG and Rolfes R 2016. An improved two-step soil-structure interaction modeling method for dynamical analyses of offshore wind turbines. *Applied Ocean Research* **55** 141-150.
[21] Hübler C, Häfele J, Gebhardt CG and Rolfes R 2018. Experimentally supported considerations of operating point dependent soil properties in coupled dynamics of offshore wind turbines. *Marine Structures* **57** 18-37.
[22] Müller K and Cheng PW 2018. A surrogate modeling approach for fatigue damage assessment of floating wind turbines. *ASME 2018 37th International Conference on Ocean, Offshore and Arctic Engineering*, June 17-22, 2018, Madrid, Spain.
[23] International Electrotechnical Commission (IEC): Wind energy generation systems - Part 3-1: Design requirements for fixed offshore wind turbines, International standard IEC 61400-3-1:2019, 2019.
[24] Müller K and Cheng PW 2018. A surrogate modeling approach for fatigue damage assessment of floating wind turbines. *ASME 2018 37th International Conference on Ocean, Offshore and Arctic Engineering*, June 17-22, 2018, Madrid, Spain.